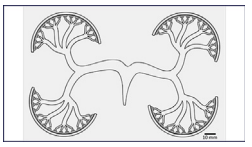

Comparison of Bolus Versus Dual-Syringe Administration Systems on Glass Yttrium-90 Microsphere Deposition in an In Vitro Microvascular Hepatic Tumor Model

Samuel R. Miller, PhD, Shaphan R. Jernigan, MS, Robert J. Abraham, MD, and Gregory D. Buckner, PhD

ABSTRACT

Purpose: To utilize an in vitro microvascular hepatic tumor model to compare the deposition characteristics of glass yttrium-90 microspheres using the dual-syringe (DS) and traditional bolus administration methods.

Materials and Methods: The microvascular tumor model represented a 3.5-cm tumor in a 1,400-cm^3 liver with a total hepatic flow of 160 mL/min and was dynamically perfused. A microcatheter was placed in a 2-mm artery feeding the tumor model and 2 additional nontarget arteries. Glass microspheres with a diameter of 20–30 μm were administered using 2 methods: (*a*) DS delivery at a concentration of 50 mg/mL in either a single, continuous 2-mL infusion or two 1-mL infusions and (*b*) bolus delivery (BD) of 100 mg of microspheres in a single 3-mL infusion.

Results: Overall, the degree of on-target deposition of the microspheres was 85% ± 11%, with no significant differences between the administration methods. Although the distal penetration into the tumor arterioles was approximately 15 mm (from the second microvascular bifurcation of the tumor model) for all the cases, the distal peak particle counts were significantly higher for the DS delivery case (approximately 5×10^5 microspheres achieving distal deposition vs 2×10^5 for the BD case). This resulted in significantly higher deposition uniformity within the tumor model (90% for the DS delivery case vs 80% for the BD case, $\alpha = 0.05$).

Conclusions: The use of this new in vitro microvascular hepatic tumor model demonstrated that the administration method can affect the deposition of yttrium-90 microspheres within a tumor, with greater distal deposition and more uniform tumor coverage when the microspheres are delivered at consistent concentrations using a DS delivery device. The BD administration method was associated with less favorable deposition characteristics of the microspheres.

ABBREVIATIONS

BD = bolus delivery, DS = dual-syringe, HCC = hepatocellular carcinoma, ID = inner diameter, PHA = proper hepatic artery, PRU = peripheral resistance units, TARE = transarterial radioembolization, ^{90}Y = yttrium-90

Transarterial radioembolization (TARE) with yttrium-90 (^{90}Y) microspheres has proven effective in controlling liver tumors and improving patient outcomes through radiation-induced cytotoxicity (1). The variables affecting procedural efficacy include average specific activity per microsphere, embolic distribution, and microvascular penetration of microspheres throughout the tumor (2). Ideally, a sufficient number of microspheres should be delivered to provide radiation coverage of all tumor cells but not so many that reflux to nontarget tissues and organs occurs (2,3). Optimizing microsphere deposition can reduce crossfire cold spots that can result in incomplete tumor destruction and continued tumor growth (4). Two studies (5,6) investigated various aspects of microsphere deposition in TARE procedures based on histologically derived distributions and aggregations of microspheres. Computational fluid dynamic studies have investigated the trajectories of resin and glass microspheres after their infusion into the hepatic arteries; several were outlined in a review by Aramburu et al (7). Although useful for predicting segment-to-segment particle depositions as a function of treatment and patient parameters, computational fluid dynamic simulations lacked the capabilities to model embolic deposition within the microvasculature. Although in vitro TARE studies (8–11) have been published in recent years, their representation of the microvasculature is limited or nonexistent, and they did

© SIR, 2022. This is an open access article under the CC BY license (http://creativecommons.org/licenses/by/4.0/).
J Vasc Interv Radiol 2023; 34:11–20
https://doi.org/10.1016/j.jvir.2022.07.032

RESEARCH HIGHLIGHTS

- An in vitro microvascular hepatic tumor model was developed and used to evaluate and compare microsphere administration methods during radioembolization procedures. The transparent planar geometry of this model enables optical assessment of microsphere distributions, and its dynamic perfusion system maintains realistic hepatic pressures and flow rates.
- The deposition characteristics of yttrium-90 glass microspheres were evaluated for 2 administration methods: conventional bolus delivery and dual-syringe delivery.
- Administration using a dual-syringe delivery device was associated with more uniform deposition of the microspheres and a higher degree of distal deposition when compared with a bolus delivery device.

STUDY DETAILS

Study type: Laboratory study

not investigate the factors affecting distal penetration and tumor coverage.

Microsphere deposition may be affected by the administration method used for delivery. The bolus delivery (BD) method for existing ^{90}Y glass TARE (TheraSphere; Boston Scientific, Marlborough, Massachusetts) requires minimum threshold pressures and flow rates to propel the glass microspheres through the delivery tubing and microcatheter. A dual-syringe (DS) administration system (ABK Biomedical, Halifax, Nova Scotia, Canada) was developed that allows for simultaneous delivery of saline and glass microspheres, enabling controlled delivery without minimum pressure or flow rate thresholds. A direct comparison of these administration methods for ^{90}Y glass microspheres has not been evaluated to date.

A new hepatic tumor vascular model was developed that replicates the anatomic features of the hepatic arterial vasculature from the proper hepatic artery (PHA) down to the tumor arteriole level. The transparent planar geometry of the tumor microvasculature enables direct microscopic evaluation of microsphere distribution, whereas the computer-controlled dynamic perfusion system allows for real-time control of hepatic pressures and flow rates. This model can be used to evaluate microsphere delivery methods prior to in vivo testing, potentially reducing or eliminating the need for animal testing in preclinical assessments. In this study, the model enabled the investigation of the effects of the 2 administration methods (BD vs DS delivery) on the deposition of glass microspheres within a simulated liver tumor.

MATERIALS AND METHODS

Institutional review board approval was not required to conduct this study.

Model Design

A 2-dimensional planar hepatocellular carcinoma (HCC) tumor model was developed to capture the key anatomic features of the human systemic vasculature while matching published physiologic pressures and flow rates throughout the branching vessels of the model. These features are summarized in the **Table** (12). Because of model size constraints, its parameters were based on an assumed tumor diameter of 3.5 cm. The total flow resistance in the target model was calculated using 2-compartment partition, which consisted of tumor and normal liver components. The tumor flow rate (Q_{tumor}) was based on the tumor volume fraction ($V_{\text{tumor}}/V_{\text{liver}}$) multiplied by the tumor-to-normal uptake ratio (T/N) and the total liver blood flow (Q_{liver}).

$$Q_{tumor} = \frac{V_{tumor}}{V_{liver}} \cdot \frac{T}{N} \cdot Q_{liver} \quad (1)$$

The total liver flow rate was assumed to be 160 mL/min based on Doppler sonography measurements, as published by Hübner et al (13). The T/N ratio was assumed to be 8:1, and the liver volume was assumed to be 1,400 mL, both within the ranges published by Ho et al (14). The tumor volume was calculated to be 22 mL by assuming spherical tumor geometry. The resulting tumor flow rate was calculated to be 20 mL/min using Equation (1). To design the tumor model, the target tumor hydraulic resistance was calculated as follows:

$$R_h = \frac{\langle P \rangle}{\langle Q \rangle} \quad (2)$$

In Equation (2), R_h is the hydraulic resistance, $\langle P \rangle$ is the time-averaged pressure, and $\langle Q \rangle$ is the time-averaged volumetric flow rate. Based on the **Table**, the average pressure in the PHA can be approximated to be 90 mmHg. Using the above equation, the target hydraulic resistance was 260 peripheral resistance units (PRU, mm Hg·s/mL).

The resulting tumor model design is shown in **Figure 1**; it consists of 4 identical microvascular trees connected by a mesoscale vascular manifold. Each microvascular tree comprises 5 branch generations, with 4–5 branches per generation. The width and length of each branch is scaled by the inverse of the branch generation. This results in a single 1-mm caliber inlet branching down to 6,400 outlet arterioles with a width of 18 μm. Additionally, the channel heights range from 370 μm in the first generation to 40 μm in the last generation, whereas the channel lengths range from 21 mm to 180 μm. This tumor model geometry results in a hydraulic resistance of 256 PRU, which is within 2% of the target resistance of 260 PRU, thus effectively replicating the pressure drop from large arteries to arterioles under physiologic flow rates.

Table. Physical Quantities for the Systemic Circulation (14)

Vessel	Diam. (mm)	Length (mm)	Number	Vol. (mL)	Area (cm^2)	Velocity (m/s)	Press. (mmHg)
Aorta	22	600	1	228	4	0.25	95
Large Arteries	6	300	40	339	11	0.083	93
Small Arteries	2	50	2400	377	75	0.012	87
Arterioles	0.02	3	1.1×10^6	104	346	0.003	54
Capillaries	0.01	1	3.3×10^9	259	2592	0.0004	25
Venules	0.04	3	2.2×10^8	829	2765	0.0003	7
Small Veins	2	50	2400	377	75	0.012	4
Large Veins	10	300	40	943	31	0.03	3
Venae Cava	22	500	2	228	4	0.25	0

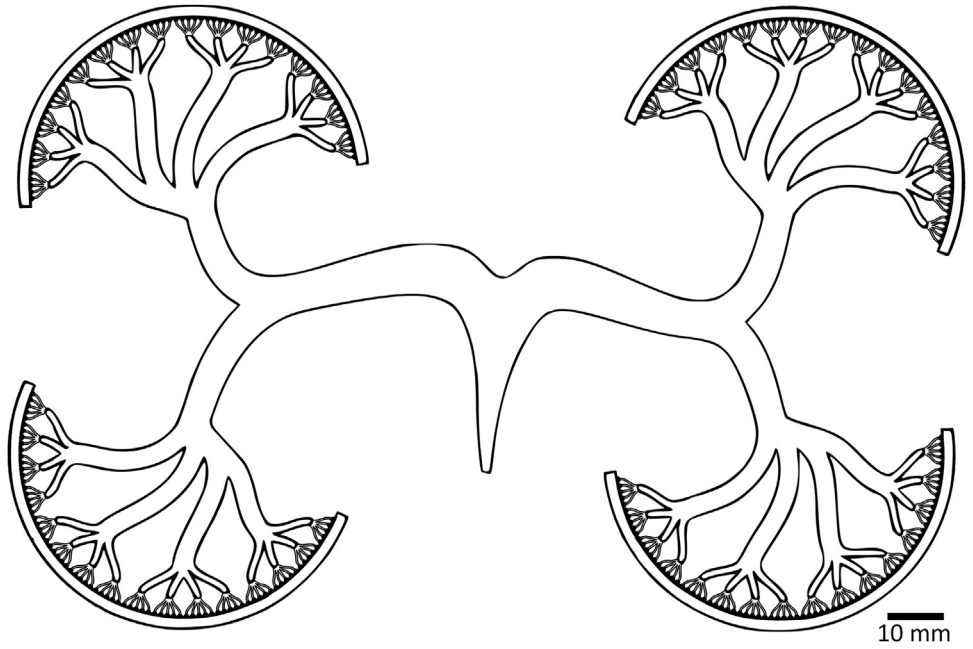

Figure 1. Microvascular tumor model design. This model consisted of 4 microvascular trees connected by a mesoscale vascular manifold. The analytical hydraulic resistance of this design was 256 peripheral resistance units, which was within 2% of the target resistance of 260 peripheral resistance units.

Microsphere Concentration

The particle concentration delivered through the microcatheter using the 2 administration methods and using either hand injection or a syringe pump was measured by collecting a continuous 10-mL infusion in 1-mL aliquots for each delivery and method, drying the aliquots in a vacuum desiccator, and massing the remaining microspheres. This was performed separately from the HCC model runs to illustrate the differences in microsphere concentration delivered in the volumes of injection between BD and DS delivery.

Microsphere Administration

To simulate a TARE procedure, the tumor model was connected to a hepatic perfusion system (Fig 2), which delivered a pulsatile flow of a water-glycerin mixture to the hepatic vascular system and tumor model. The ratio of water to glycerin was tuned to approximate the dynamic viscosity of whole blood at 3.5 cP (9). The hepatic vascular system (Fig 3) consisted of the PHA, which bifurcated into the left and right hepatic arteries. The left and right hepatic arteries branched down to 16 outlet arteries with an inner diameter (ID) of 1 mm. The flow rate in the PHA was set to approximately 160 mL/min at a pressure of 140/60 mm Hg. The flow rate in the PHA was tuned by adjusting the length of the 1-mm-ID outlet arteries to achieve an average flow rate of approximately 10 mL/min for each outlet. The tumor model was attached to 1 of the 16 outlet arteries originating from a 2-mm caliber artery. Microspheres were administered through a 2.9-F (ID, 0.027 inch), 150-cm Cook Cantata microcatheter (Cook Medical, Bloomington, Indiana), which had been placed into the 2-mm caliber artery feeding the tumor model and 2 adjacent outlet arteries, simulating segmental therapy. The adjacent outlet arteries represent small arteries feeding normal liver

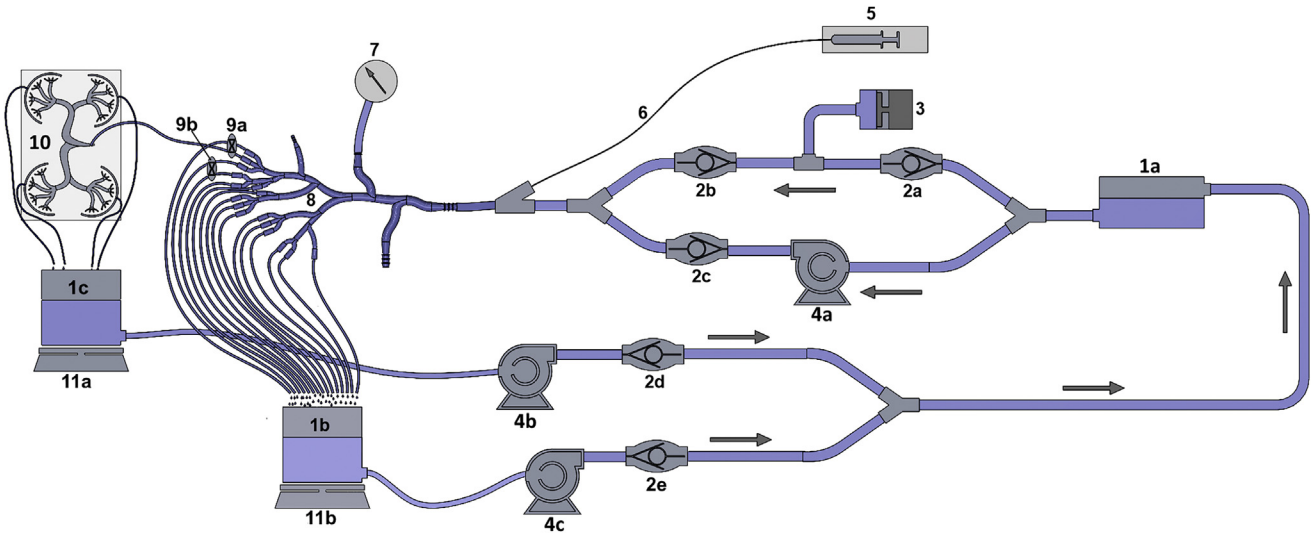

Figure 2. A schematic of the hepatic perfusion system. 1a–1c = reservoirs; 2a–2e = 1-way check valves; 3 = pulsatile pump; 4a–4c = centrifugal pumps; 5 = syringe pump; 6 = delivery catheter; 7 = pressure transducer; 8 = hepatic vascular system; 9a and 9b = pinch valves; 10 = tumor model; 11a and 11b = digital scales.

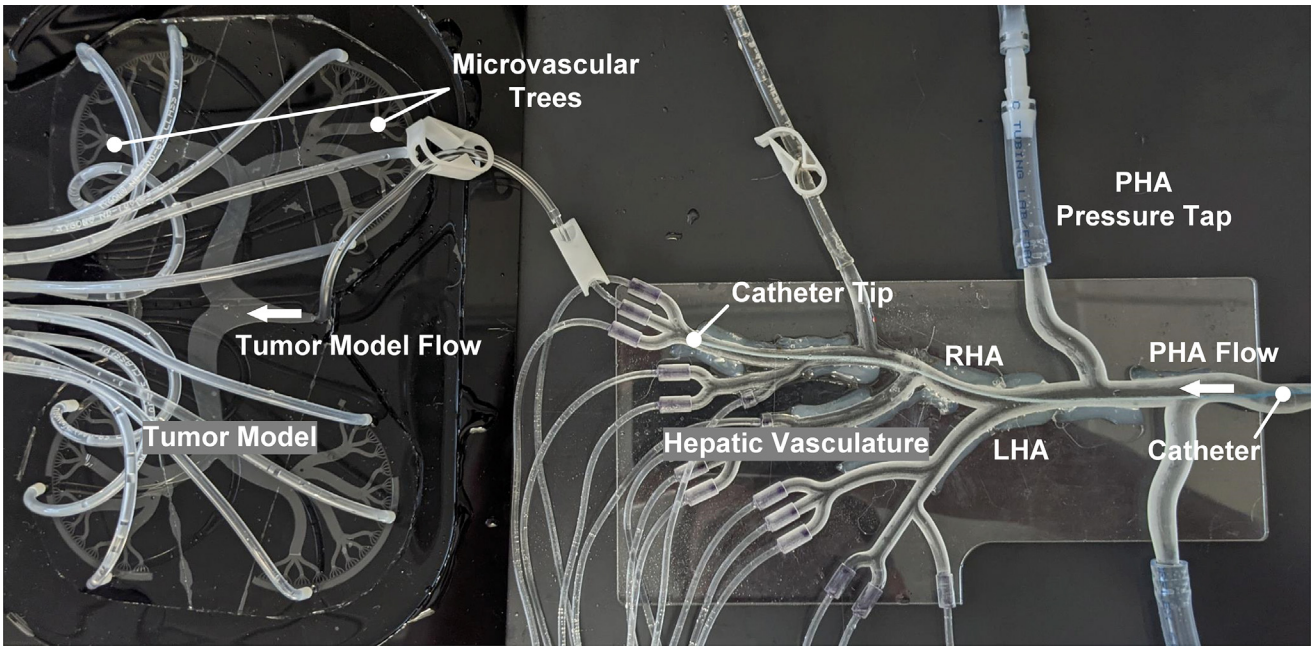

Figure 3. An overview of the experimental microsphere administration setup showing the tumor model connected to the hepatic vascular system. LHA = left hepatic artery; PHA = proper hepatic artery; RHA = right hepatic artery.

tissue, to which the catheter could not be placed distally because of artery size restrictions. The *T*/*N* ratio of 8:1 was approximated using pinch valves to limit the flow rate in the adjacent outlet arteries to 2.5 mL/min each (one eighth of a theoretical tumor model flow rate of 20 mL/min).

Two different delivery devices were used to administer approximately 100 mg of yttrium-89 glass microspheres with a diameter of 20–30 μm (ABK Biomedical) through the microcatheter: a DS system (ABK Biomedical) and a BD system that was functionally equivalent to commercially available delivery systems for ^{90}Y glass microspheres (Fig 4). The DS system consisted of 2 syringes actuated in parallel to deliver a relatively constant microsphere concentration of up to 50 mg/mL throughout administration. Two cases were evaluated using the DS device: (*a*) continuous administration of a 2-mL infusion at a rate of 0.3 mL/s and (*b*) intermittent administration of two 1-mL infusions at a rate of 0.3 mL/s with a 3-minute pause in between. One case was tested using the BD

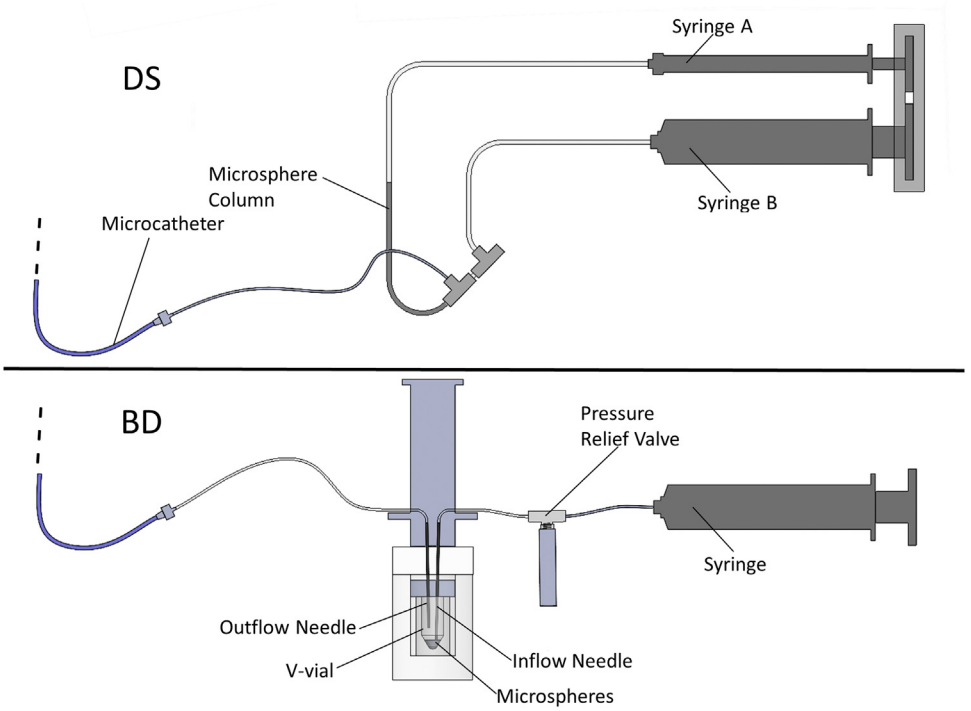

Figure 4. A schematic of the dual-syringe and bolus delivery administration methods. BD = bolus delivery; DS = dual-syringe.

system: a single, continuous 3-mL BD at a rate of 0.6 cm^3/s. The administration rate of 0.6 mL/s was chosen to ensure that enough pressure was applied to the BD system to properly agitate the microspheres within the v-vial while producing slow drip from the system's pressure-relief valve.

The trials were conducted by introducing the microcatheter through a Tuohy-Borst valve as shown in **Figure 2** and placing the tip within the 2-mm caliber artery, as shown in **Figure 3**. The microspheres were administered using a computer-controlled syringe pump to actuate either the DS or BD system under previously specified case parameters. Following administration, the system was allowed to perfuse for 5 minutes to ensure that microsphere deposition was complete. Next, the catheter was removed, the flow rates were again allowed to reach a steady state, and the final postembolization flow rates were recorded. Finally, the pinch valve was closed to stop flow to the tumor model, which was then disconnected from the hepatic vascular system and subsequently imaged using a computer-controlled microscope camera. Nontarget microspheres were collected from a filter at the outlet hepatic arteries, rinsed in water, dried, and massed. Remnant microspheres remaining in the catheter and delivery devices were also massed. The on-target microsphere mass was calculated by subtracting the nontarget and remnant microsphere masses from the total mass prepared for each trial. The model pressures and flow rates, microsphere concentration emitted from the catheter tip, total particle count across all microvascular trees, assessment of on-target or nontarget deposition, and distal penetration were evaluated and compared between the BD and DS groups.

Statistical Analyses

Statistical analyses were conducted using MATLAB Statistics and Machine Learning Toolbox (The MathWorks, Natick, Massachusetts). The differences in sample means were tested using the analysis of variance, with multiple comparisons being computed using the Tukey honestly significant difference test, with a significance level of $\alpha = 0.05$. A sample size of 4 was used for all the cases. All error bars indicate the standard error of the mean. Sample means and standard deviations are notated as mean ± standard deviation.

RESULTS

Model Parameters

The measurements of the model pressures and flow rates prior to catheter placement showed that with an average pressure of 90 mm Hg, the model yields an actual resistance of 222 PRU, which is within 15% of the target resistance of 260 PRU. Prior to administration, the microsphere concentrations emitted from the catheter tip were measured for both the administration methods. The BD method resulted in peak microsphere concentrations of as high as 100 mg/mL compared with the 50-mg/mL concentration for the DS method.

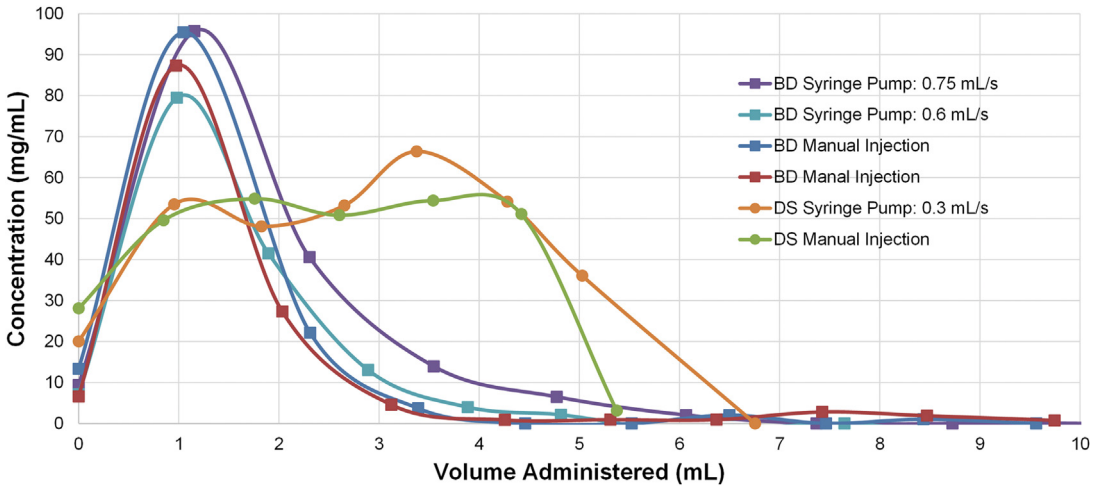

Figure 5. Microsphere concentration versus administered volume for hand injection-delivered and syringe pump-delivered bolus delivery and dual-syringe delivery. BD = bolus delivery; DS = dual-syringe.

Microsphere Concentration

BD via hand injection or the syringe pump showed early high microsphere concentration peaks, with a relatively quick drop in concentrations, in comparison with DS injection, which showed a slower rise to peak and a longer time at a relatively steady plateau (Fig 5).

Microsphere Distribution

Figure 6 shows an example of the tumor model following embolization. Here, microsphere depositions can be seen in the microvascular trees (numbered and highlighted in purple) and proximal mesoscale vasculature (highlighted in yellow). The purple microvascular regions were scanned using the aforementioned microscope imaging system; more proximal regions, such as the mesoscale vasculature, highlighted in yellow, were not scanned and were not included in the quantification of distribution. A higher-magnification comparison of microsphere distributions (in identical portions of Microvascular Tree 1) for each administration method is provided in Figure 7. Here, the DS cases reveal more distal filling of the vasculature, whereas the BD case shows significant proximal accumulation. It should be noted that at least some microspheres reached the most distal microvascular branches in every case, although these distal microspheres are difficult to visualize in Figure 7 because of their size.

Particle counting across all microvascular trees was accomplished using custom image processing algorithms of digital micrographs; the mean particle counts are summarized in Figure 8. Here, the 2-way analysis of variance revealed that the administration method significantly impacts particle deposition count, although there was no significant dependence on vascular trees or interaction between variables.

Although Figure 8 reveals variation in the particle counts of adjacent microvascular trees (Trees 1–4),

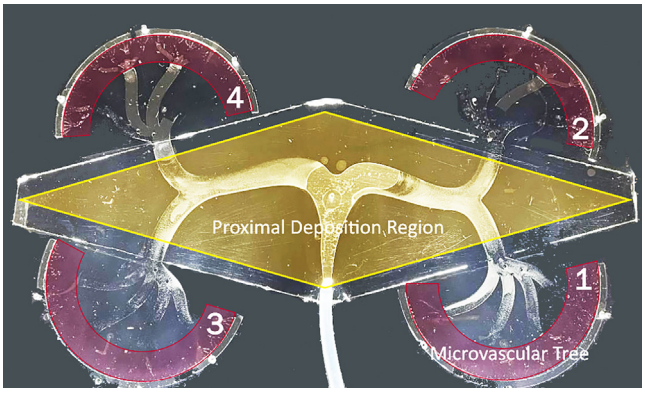

Figure 6. A photograph of an embolized microvascular tumor model administered using bolus delivery. Here, the purple annotated regions indicated the microvascular branches scanned using the microscope imaging system; more proximal regions, including the mesoscale vasculature, highlighted in yellow, had microsphere depositions that were not quantified using the imaging system.

Figure 9 indicates that the total on-target deposition particle mass was not significantly different across all the test cases. This is likely because the BD case exhibited noticeable accumulation of microspheres in regions proximal to the microvascular trees; these microspheres were not counted but did contribute to the on-target particle mass. Overall, there was a high degree of on-target deposition (on-target mass fraction, 85% ± 11%), with no significant differences in either on-target or nontarget deposition across both the test groups (Fig 9). On average, 78.7 mg ± 18.7 of microspheres were delivered through the microcatheter in both groups. The uniformity of microsphere deposition for each case was calculated as the percent difference between ideal uniformity (where each of the 4 microvascular trees accumulates 1 quarter of the total particle count) and measured totals; thus, a uniformity of

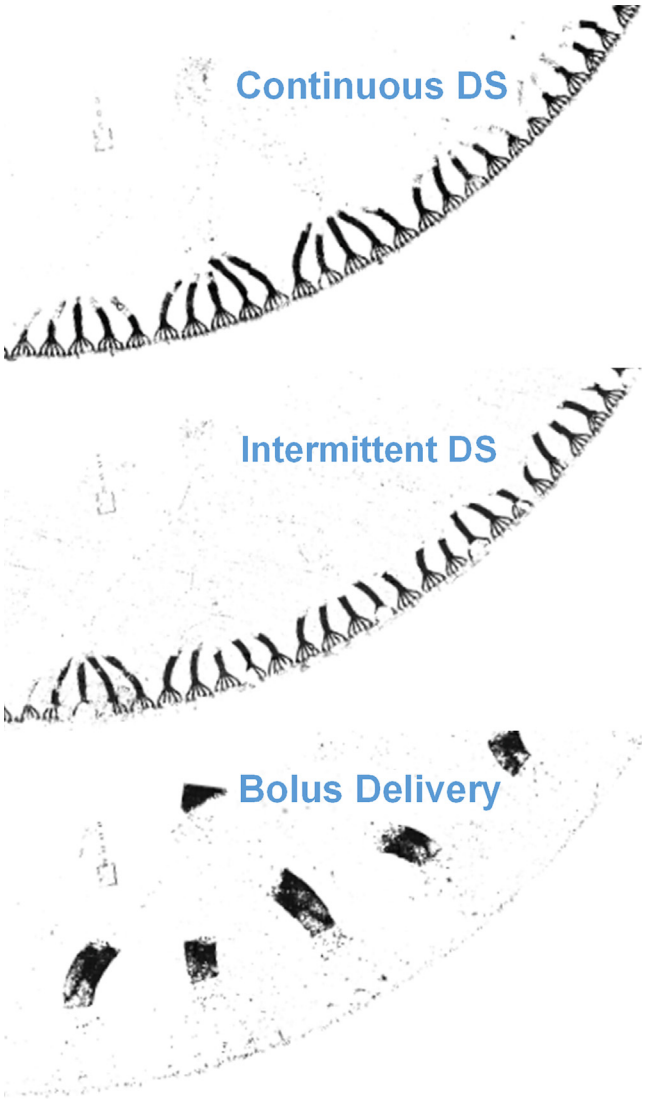

Figure 7. Sample particle distributions in Microvascular Tree 1 for the continuous dual-syringe (top), intermittent dual-syringe (middle), and bolus delivery cases (bottom). DS = dual-syringe.

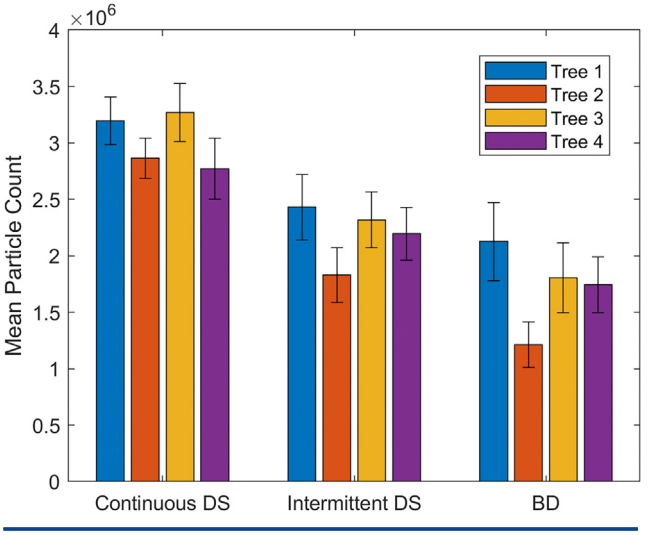

Figure 8. Microsphere count by microvascular tree. BD = bolus delivery; DS = dual-syringe.

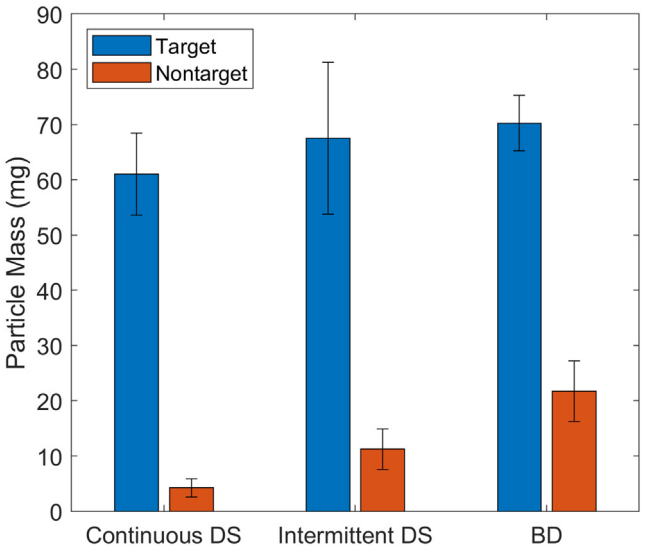

Figure 9. Total target and nontarget microsphere deposition within the entire model. BD = bolus delivery; DS = dual-syringe.

1.0 indicates that each microvascular branch had the same measured particle count. **Figure 10** shows the average uniformity for each test case, with the BD case showing significantly lower uniformity than the other cases.

For this study, distal penetration was statistically defined as the radial distance into the microvasculature (from the second microvascular bifurcation of each tree in the tumor model: the proximal boundaries of the purple regions in **Fig 6**) achieved by 95% of the microspheres. Thus, for each test case, 5% of the microspheres deposited within the microvasculature were observed even more distally. **Figure 11** shows that the distal penetration for each case was approximately 15 mm, although the distribution magnitudes were very different, as shown in **Figure 12**. Here, 2 distinct peaks were generally observed: a distal peak at 14 mm and a smaller, more proximal peak at approximately 8–12 mm. The BD case showed a smaller distal peak of approximately 2×10^5 microspheres versus the DS cases, which had a distal peak of approximately 5×10^5, indicating that far fewer particles reached the microvasculature (ie, they were deposited proximally in the mesoscale vasculature) in the BD case.

DISCUSSION

The design and fabrication methods resulted in a model with the measured flow resistance within 15% of the target theoretical resistance, validating the design assumptions (laminar flow, etc) and providing realistic pressures and flow rates. The average microsphere administration of 78.7

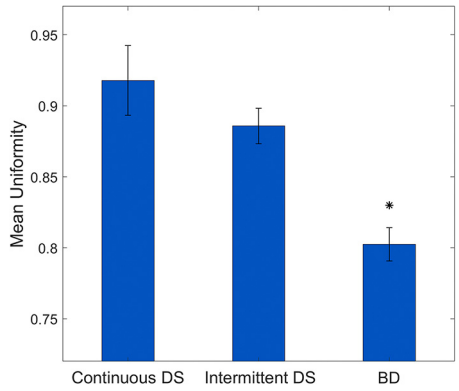

Figure 10. The uniformity of mean microsphere deposition across microvascular trees. Here, 1.0 represents total uniformity, indicating that each of the 4 microvascular trees received the same number of microspheres. BD = bolus delivery; DS = dual-syringe. *The bolus delivery case showed significantly (α = 0.05) lower uniformity than either DS case.

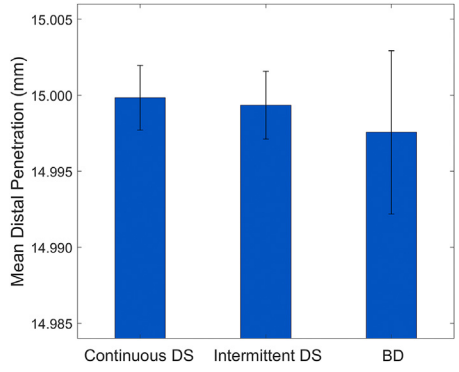

Figure 11. Mean distal penetration (from the second microvascular bifurcation of the tumor model) into the outlet arteriole flow channels. BD = bolus delivery; DS = dual-syringe.

mg resulted in an average on-target deposition of 85%, with the remainder being collected from adjacent nontarget arteries. Although there were no significant differences between on- and off-target depositions between both groups, some variations were observed in the measured particle counts between adjacent microvascular trees. As stated previously, the lower particle counts for the BD case were a result of particle accumulations within the tumor model proximal to the microvascular trees. This shows that the gross distributions within the model (proximal vs distal) were noticeably different, with the continuous and intermittent DS cases showing mostly distal deposition in the microvascular trees of the tumor model.

This observation was further recapitulated at the microvascular scale, where the most distal peak particle count was approximately 3-fold higher for the DS cases than for the BD case. This difference in distal distributions is visually evident in Figure 7, where most distal microchannels were filled with microspheres for the DS cases. In contrast, the BD case revealed less filling of distal channels and distinct proximal accumulations in contrast to the continuous and intermittent DS cases. It should be noted that no significant differences were observed in distal penetration across all the cases, indicating that it is largely a function of microsphere size, with flow parameters (pressure, velocity, etc) likely having a more subtle effect.

These observations indicate that the administration method does significantly affect the number of particles reaching the distal microvasculature, with BD showing less favorable distal distributions. One major factor affecting the BD case is its administration flow rate relative to the tumor flow rate. The results indicate that during BD administration, there is greater back pressure in the tumor, resulting in a significant reduction of the tumor flow rate. This reduction of the flow rate while particles are being deposited within the tumor likely causes the microspheres to accumulate prematurely rather than remain in the flow until they reach the target distal microvasculature. More gradual administration in the intermittent and continuous DS cases results in minimal reduction of tumor flow during deposition, allowing particles to reach the distal microvasculature.

With regard to lateral deposition, there were no significant differences between the particle counts in the 4 microvascular trees for any given administration method. However, when complete uniformity was compared (all 4 microvascular trees receiving the same number of microspheres), some significant differences were observed. The results indicate that the average uniformity was significantly lower for the BD case than for all the other cases. This observation could be a consequence of particle-laden flow during peak bolus concentration. Such flows have been shown to exhibit nontypical behaviors, such as preferential concentration of particles within turbulent regions and changes in bulk flow characteristics (such as density and resistance) (15). These effects, especially preferential concentration, could explain why BD administration showed lower average uniformity than the DS cases.

When the intermittent and continuous DS cases were compared, no significant differences were seen. This suggests that there are no advantageous or detrimental effects caused by pausing administration to conduct intraprocedural C-arm cone-beam computed tomography imaging. From these comparisons alone, it is not clear whether intermittent administration in the BD case would have benefited its response. As previously hypothesized, a high administration rate relative to the pre-embolization tumor flow rate resulted in more proximal deposition and less lateral uniformity. By introducing a pause during administration, the average administration rate can be reduced, possibly resulting in greater distal deposition and improved lateral uniformity. Additional studies should be conducted to fully understand the effect of intermittent administration, its relevant parameters (flow rate, pause duration, delivery device, etc), and its potential impact on clinical outcomes.

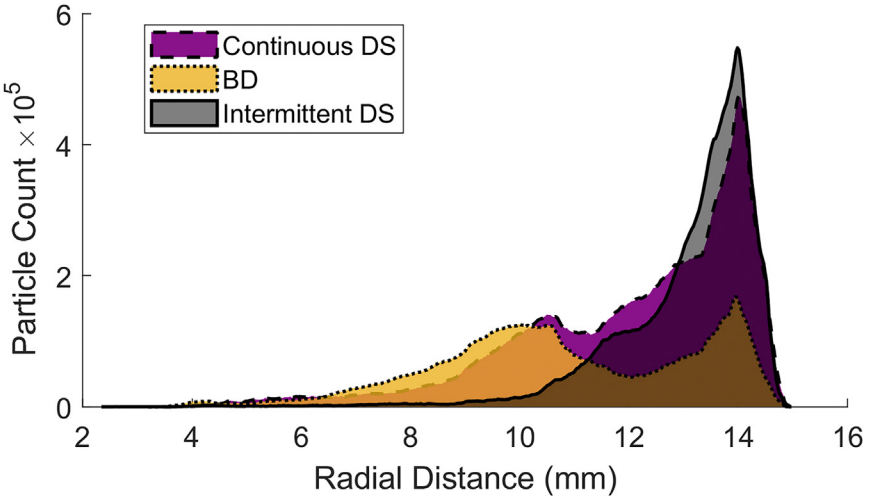

Figure 12. Mean microsphere count by radial distance measured from the second microvascular bifurcation of the tumor model. BD = bolus delivery; DS = dual-syringe.

A microscopic analysis using this in vitro tumor model revealed that the administration method had a noticeable effect on distal microsphere distribution. Administration using the DS delivery device was associated with a higher degree of distal deposition than that using the BD system. Furthermore, DS administration resulted in more uniform tumor coverage with the microspheres compared with bolus administration. The results of this study indicate that the administration method may affect clinical outcomes and could be attributable to the differences in microsphere concentrations during administration. Specifically, BD is associated with a higher peak concentration, occurring early during administration, followed by rapid reduction. On the contrary, DS delivery yields more gradual onset of concentration, with a relative plateau of concentration for several seconds. These results also highlight the high level of detail with which embolic microparticle deposition can be evaluated using this type of vascular model. Although not a substitute for animal or human clinical trials, the tumor model and the conclusions of this study can be used to inform current practice and future clinical studies as well as support rapid technological innovation of new embolics, delivery devices, and administration methods.

The limitations of this study include the relatively small sample sizes, 2-dimensional planar geometry of the in vitro tumor model, limited administration parameters used, and lack of clinical validation. Because a large range of *T/N* ratios have been observed in patients with HCC (13), a range of tumor flow rates should be evaluated in the future to understand its effect on microsphere deposition. Additionally, varying administration rates and microcatheter tip positions should be studied to determine how this factor can influence distal deposition and the uniformity of coverage in HCC tumors.

ACKNOWLEDGMENTS

This work was performed in part at the North Carolina State University Nanofabrication Facility, a member of the North Carolina Research Triangle Nanotechnology Network, which is supported by the National Science Foundation (Grant ECCS-1542015) as part of the National Nanotechnology Coordinated Infrastructure. This study was funded in part by ABK Biomedical Inc., which is developing products related to the research described in this paper.

AUTHOR INFORMATION

From the Department of Mechanical and Aerospace Engineering (S.R.M., S.R.J., G.D.B.), North Carolina State University, Raleigh, North Carolina; Department of Diagnostic Radiology (R.J.A.), Dalhousie University, Halifax, Nova Scotia, Canada; and ABK Biomedical Inc. (R.J.A.), Halifax, Nova Scotia, Canada. Received December 14, 2021; final revision received July 12, 2022; accepted July 17, 2022. Address correspondence to R.J.A., Department of Diagnostic Radiology, Dalhousie University, 1276 South Park Street, Room 307, Halifax, NS B3H 2Y9, Canada; E-mail: robert.abraham@dal.ca

R.J.A. is the cofounder, a shareholder, and an employee (Chief Medical Officer) of ABK Biomedical Inc.; was involved with protocol development, data analysis, review, and editing of the manuscript; and received funding for the research conducted as well as bland and ^{90}Y radiopaque microspheres and microsphere delivery systems from ABK Biomedical Inc. G.D.B. received funding from ABK Biomedical Inc. to conduct this study. None of the other authors have identified a conflict of interest.

From the Global Embolization Symposium & Technologies 2021, "Novel hepatic tumor microvascular model for evaluating the embolic charactersitics of Y-90 microspheres." J Vasc Interv Radiol, 2021; 32(8): e33-e53

REFERENCES

1. Westcott MA, Coldwell DM, Liu DM, Zikria JF. The development, commercialization, and clinical context of yttrium-90 radiolabeled resin and glass microspheres. Adv Radiat Oncol 2016; 1:351–364.
2. Rose SC, Narsinh KH, Isaacson AJ, Fischman AM, Golzarian J. The beauty and bane of pressure-directed embolotherapy: hemodynamic principles and preliminary clinical evidence. AJR Am J Roentgenol 2019; 212:686–695.
3. Kennedy A, Coldwell D, Sangro B, Wasan H, Salem R. Radioembolization for the treatment of liver tumors general principles. Am J Clin Oncol 2012; 35:91–99.

4. Morgan B, Kennedy AS, Lewington V, Jones B, Sharma RA. Intra-arterial brachytherapy of hepatic malignancies: watch the flow. Nat Rev Clin Oncol 2011; 8:115–120.
5. Kennedy AS, Nutting C, Coldwell D, Gaiser J, Drachenberg C. Pathologic response and microdosimetry of (90)Y microspheres in man: review of four explanted whole livers. Int J Radiat Oncol Biol Phys 2004; 60: 1552–1563.
6. Bilbao JI, de Martino A, de Luis E, et al. Biocompatibility, inflammatory response, and recannalization characteristics of nonradioactive resin microspheres: histological findings. Cardiovasc Intervent Radiol 2009; 32:727–736.
7. Aramburu J, Antón R, Rodríguez-Fraile M, Sangro B, Bilbao JI. Computational fluid dynamics modeling of liver radioembolization: a review. Cardiovasc Intervent Radiol 2022; 45:12–20.
8. Richards AL, Kleinstreuer C, Kennedy AS, Childress E, Buckner GD. Experimental microsphere targeting in a representative hepatic artery system. IEEE Trans Biomed Eng 2012; 59:198–204.
9. Jernigan SR, Osborne JA, Mirek CJ, Buckner G. Selective internal radiation therapy: quantifying distal penetration and distribution of resin and glass microspheres in a surrogate arterial model. J Vasc Interv Radiol 2015; 26:897–904.
10. van den Hoven AF, Lam MG, Jernigan S, van den Bosch MA, Buckner GD. Innovation in catheter design for intra-arterial liver cancer treatments results in favorable particle-fluid dynamics. J Exp Clin Cancer Res 2015; 34:1–9.
11. Caine M, McCafferty MS, McGhee S, et al. Impact of yttrium-90 microsphere density, flow dynamics, and administration technique on spatial distribution: analysis using an in vitro model. J Vasc Interv Radiol 2017; 28:260–268.
12. Hoskins PR. Introduction to cardiovascular biomechanics. In: Hoskins PR, Lawford PV, Doyle BJ, editors. *Cardiovascular Biomechanics*. Cham: Springer International Publishing; 2017. p. 25–35.
13. Hübner GH, Steudel N, Kleber G, Behrmann C, Lotterer E, Fleig WE. Hepatic arterial blood flow velocities: assessment by transcutaneous and intravascular Doppler sonography. J Hepatol 2000; 32:893–899.
14. Ho S, Lau WY, Leung TW, et al. Partition model for estimating radiation doses from yttrium-90 microspheres in treating hepatic tumours. Eur J Nucl Med 1996; 23:947–952.
15. Tabaeikazerooni SH. Laminar and turbulent particle laden flows: a numerical and experimental study. Available at: http://urn.kb.se/resolve?urn=urn:nbn:se:kth:diva-250801. Accessed October 21, 2021.